Mechanisms of Cardiac Cell Excitation with Premature Monophasic and Biphasic Field Stimuli: A Model Study

Matthew G. Fishler, Eric A. Sobie, Nitish V. Thakor, and Leslie Tung
The Johns Hopkins University School of Medicine, Department of Biomedical Engineering, Baltimore, Maryland 21205 USA

ABSTRACT   The mechanisms by which extracellular electric field stimuli induce the (re)excitation of cardiac cells in various stages of refractoriness are still not well understood. We modeled the interactions between an isolated cardiac cell and imposed extracellular electric fields to determine the mechanisms by which relatively low-strength uniform monophasic and biphasic field stimuli induce premature reexcitations. An idealized ventricular cell was simulated with 11 subcellular membrane patches, each of which obeyed Luo-Rudy (phase 1) kinetics. Implementing a standard S1–S2 pulse protocol, strength-interval maps of the cellular excitatory responses were generated for rectangular monophasic and symmetric biphasic field stimuli of 2, 5, 10, and 20 ms total duration. In contrast to previously documented current injection studies, our results demonstrate that a cardiac cell exhibits a significantly nonmonotonic excitatory response to premature monophasic and, to a much lesser degree, biphasic field stimuli. Furthermore, for monophasic stimuli at low field strengths, the cell is exquisitely sensitive to the timing of the shock, demonstrating a classic all-or-none depolarizing response. However, at higher field strengths this all-or-none sensitivity reverts to a more gradual transition of excitatory responses with respect to stimulus prematurity. In contrast, biphasic stimuli produce such graded responses at all suprathreshold stimulus strengths. Similar behaviors are demonstrated at all S2 stimulus durations tested. The generation of depolarizing (sodium) currents is triggered by one or more of the sharp field gradient changes produced at the stimulus edges—i.e., make, break, and transphasic (for biphasic stimuli)—with the magnitude of these edge-induced current contributions dependent on both the prematurity and the strength of the applied field. In all cases, however, depolarizing current arises from the partial removal of sodium inactivation from at least part of the cell, because of either the natural process of repolarization or a localized acceleration of this process by the impressed field.

INTRODUCTION

Cardiac cells can be stimulated either via intracellular current injection or via an applied extracellular electric field. In the former method, positive current is injected into the cell via an intracellularly situated electrode (such as a perforated patch pipette), uniformly driving the entire cell's transmembrane voltage above its threshold value. In contrast, during field stimulation, no net current is introduced into the cell; rather, the cell generates its own depolarizing currents (Tung and Borderies, 1992; Leon and Roberge, 1993; Krassowska and Neu, 1994). During extracellular field stimulation, a potential gradient is imposed between the anodal and cathodal electrodes, inducing an associated extracellular current flow. However, because a cell membrane is relatively nonconducting, very little of this stimulus current actually flows *through* the cell. Instead, the inside of the cell remains essentially isopotential (Knisley et al., 1993; Leon and Roberge, 1993; Krassowska and Neu, 1994). (Actually, large deviations from isopotentiality can develop intracellularly during the first few microseconds after the field is initially switched on or off (Krassowska and Neu, 1994; Fishler, manuscript submitted for publication). At these

transitions, the reactive component of the membrane impedance causes the membrane to become essentially transparent to this high-frequency current flow. However, because this effect lasts for such a short duration, it has little impact on the developing membrane dynamics (Krassowska and Neu, 1994).)

Consequently, a spatial variation in transmembrane potential develops along the cell surface, with the cell membrane nearest the anode experiencing the most significant hyperpolarization and the cell membrane nearest the cathode experiencing the most significant depolarization. Indeed, several theoretical models (Klee and Plonsey, 1976; Plonsey and Barr, 1986a; Krassowska et al., 1987; Tung and Borderies, 1992; Leon and Roberge, 1993; Krassowska and Neu, 1994) and experimental investigations (Gross et al., 1986; Windisch et al., 1992; Knisley et al., 1993) have supported the expectations of such nonuniform polarization of cells exposed to an external electric field. Furthermore, simulations of resting cells incorporating active membrane dynamics (Tung and Borderies, 1992) have shown that these oppositely polarized regions can work synergistically to bring the entire cell to threshold.

Clinically, field stimulation is extremely relevant for defibrillation and cardioversion, in which a large external shock is delivered across the myocardial volume in an attempt to extinguish potentially fatal self-sustaining arrhythmias (e.g., fibrillation or tachycardia). Moreover, with the advent of the implantable cardioverter-defibrillator (Mirowski, 1985), there has been a concerted research effort to

increase the lifetimes of these devices by improving their shock efficacy and efficiency. One improvement that has proved to be quite effective in both experimental and clinical settings is the use of biphasic (BP) stimulating waveforms instead of the more traditional monophasic (MP) waveforms (Schuder et al., 1983; Fain et al., 1989; Flaker et al., 1989; Tang et al., 1989; Winkle et al., 1989; Wharton et al., 1990). Yet, the mechanisms by which these BP waveforms outperform their MP counterparts are still unresolved. A leading hypothesis, as first suggested by Jones et al. (1987), proposes that the first phase of a BP waveform acts as a conditioning prepulse that enhances and/or reestablishes sodium channel activation, reduces the excitation threshold for the second phase of the waveform, and thus leads to improved action potential prolongation. However, their computational investigations of this hypothesis used only current injection models (Jones and Jones, 1990; Jones et al., 1994), and thus the extrapolation of those results to the more clinically relevant case of field stimulation remains in question. Indeed, only recently have such computational studies of the field stimulation of cardiac cells been published (Tung and Borderies, 1992; Leon and Roberge, 1993; Krassowska and Neu, 1994; Fishler et al., 1995). Yet, none of these studies investigated the mechanisms of field-induced excitation at different phases of cellular refractoriness and at different stimulus strengths. For example, Tung and Borderies (1992), using a three-patch model of a cardiac cell, compared the cellular and subcellular current and voltage dynamics leading to excitation via current injection and uniform MP and BP field stimulation, but only for cells at rest. Leon and Roberge (1993) implemented a 48-patch model to explore excitation efficacies of premature and nonuniform field stimuli. And Krassowska and Neu (1994) used dimensional analysis and singular perturbation theory to develop a new theoretical approach for the study of such field stimulation of cells.

In this paper, we use a computational model of an idealized isolated cardiac cell to study how both stimulus strength and prematurity influence the underlying mechanisms of field-induced excitation produced by both MP and BP extracellular field stimuli. The primary objective is to improve our fundamental understanding of the complex mechanisms of field stimulation and to add to our understanding of how and why BP waveforms may outperform similar MP shocks. Although this study focuses on single-cell events, these results may also be applicable to larger scale events as well (up to some spatial limit) in which oppositely polarized regions are in close proximity to one another (e.g., dogbone, sawtooth, etc.).

MATERIALS AND METHODS

Model description

This model simulates the active response of a single isolated cardiac cell, situated within an otherwise unbounded volume conductor, and subject to a uniform extracellular electric field stimulus. A detailed description of the

construction of the model has been published previously (Tung and Borderies, 1992).

For this study, we assume that a cardiac cell can be idealized as a prolate spheroid with a semimajor-to-semiminor axis ratio of 5:1, and that the imposed extracellular field is aligned with the cell's semimajor axis (Fig. 1 A). As such, all induced cellular dynamics are radially symmetric about the semimajor axis. Thus, this system can be adequately represented by a finite one-dimensional cable model. Further simplifications are possible by assuming that the intracellular and extracellular volumes remain spatially (but independently) isopotential in the absence of any stimulus; that is, any axial potential drops induced by axial currents are negligible when compared to the associated transmembrane voltages involved. Moreover, we also assume that no potential gradients develop within the intracellular volume during an extracellular field stimulus. This latter simplification is an approximation based on observations made in other theoretical (Klee and Plonsey, 1976; Leon and Roberge, 1993; Krassowska and Neu, 1994) and experimental (Knisley et al., 1993) studies which demonstrated that, because of the insulating nature of the cell membrane, intracellular potential gradients remain minimal, even during an extracellular field stimulus. Fig. 1 B illustrates the equivalent lumped membrane model used for these simulations, in which the cell has been subdivided into 11 discrete isopotential membrane patches (M1 through M11), and the extracellular field has been incorporated as time-dependent extracellular surface potentials, V_a, interspersed between adjacent extracellular nodes (Tung and Borderies, 1992). As mentioned above, the entire intracellular volume shares a com-
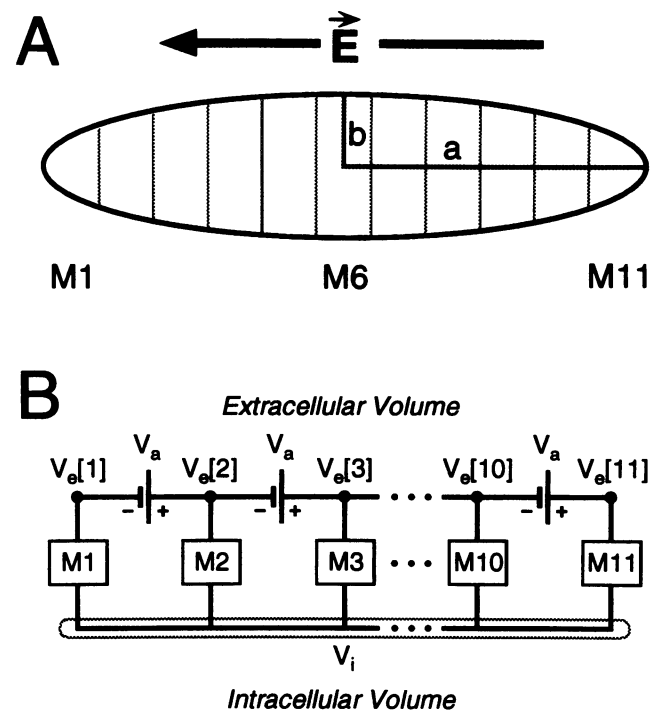

FIGURE 1 Schematic representations of a single isolated cardiac cell in a uniform extracellular electric field. (A) The simulated cell is idealized as a prolate spheroid ($a/b = 5$) subdivided into 11 discrete isopotential membrane patches, M1–M11. The surrounding unbounded extracellular volume supports an imposed uniform electric field, $\vec{E}$, oriented parallel to the long axis of the cell. (B) Equivalent one-dimensional lumped membrane cable representation of cell. The entire intracellular volume is approximated to be spatially isopotential with potential V_i, although the ionic dynamics of individual membrane patches remain independent. Extracellular potentials, $V_e[1]$ through $V_e[11]$, also remain distinct so as to be able to accommodate a field-induced spatial potential gradient along the cell surface. This gradient is implemented using extracellular boundary potentials, V_a, interspersed between adjacent extracellular nodes.

mon potential, V_i. In contrast, the extracellular nodal potentials (V_e) remain distinct so as to accommodate a (discrete) field-induced gradient along the cell surface. Transmembrane voltages are calculated for each patch as $V_m[k] = V_i - V_e[k]$ ($k = 1, 2, \ldots, 11$).

Membrane patches independently obey Luo-Rudy (phase 1) kinetics (Luo and Rudy, 1991), a quantitative model based on recent single-cell and single-channel experimental data that simulates the transmembrane ionic dynamics of mammalian cardiac ventricular cells. Temporal changes in V_i (and hence in V_m) are computed from the weighted sum over all membrane patches of the associated capacitive and transmembrane ionic currents, with weights determined by the fractional membrane surface area of each patch (Tung and Borderies, 1992).

Model implementation

This model was implemented within the Advanced Continuous Simulation Language (ACSL; Mitchell and Gauthier Associates, Concord, MA) programming environment on a Silicon Graphics (Mountain View, CA) POWER Challenge XL minisupercomputer. Membrane kinetics (Luo and Rudy, 1991) were computed using a second-order Runge-Kutta-Fehlberg algorithm with adaptive time stepping, constrained such that relative errors in the state variables remained less than 10^{-6}.

The purpose of this study was to examine the mechanisms of cellular excitation by various premature MP and BP uniform field stimuli. To do so, we implemented a standard S1-S2 pulse protocol and recorded for subsequent analysis the induced subcellular temporal changes in elemental transmembrane potentials and currents as well as sodium activation and inactivation gating kinetics. The quiescent cell was first excited by a 5-ms, 1.5× threshold, MP field stimulus (S1). Then, after a specified delay, a test field stimulus (S2) was administered across the cell. We effectively explored a three-dimensional state space of test stimuli, with variations in S2 wave shape, S2 strength, and S1-S2 coupling interval. S2 wave shapes were either rectangular MP field or symmetric BP field stimuli of 2, 5, 10, or 20 ms total duration. Tested S2 strengths ranged from 0.750× to 2.625× MP diastolic threshold, and S1-S2 coupling intervals, as measured from the S1 and S2 leading edges, ranged from 280 to 420 ms.

RESULTS

The results that we obtained for S2 stimuli of 2, 5, 10, and 20 ms total duration were qualitatively similar in terms of both general behavior and underlying mechanisms. Therefore, we present below detailed results for only the 20-ms MP and the 10/10-ms BP S2 field stimuli, so chosen for their long durations, which maximize the separation between edge-induced stimulus events (see below). A subsequent section compares results obtained for all MP and BP S2 stimuli.

Monophasic field stimulation

Fig. 2 depicts two representative responses of transmembrane potentials (V_m) from each of the 11 subcellular elements during two separate field stimulation trials. Using identical 20-ms MP field stimuli at 2× diastolic threshold, these two trials differed only in the S1-S2 coupling interval with which the field stimulus (S2) was administered: 340 ms in trial A, and 380 ms in trial B. As expected from previous works (Klee and Plonsey, 1976; Plonsey and Barr, 1986a; Krassowska et al., 1987; Tung and Borderies, 1992; Knisley et al., 1993; Leon and Roberge, 1993; Krassowska and Neu, 1994), common to both responses is a significant
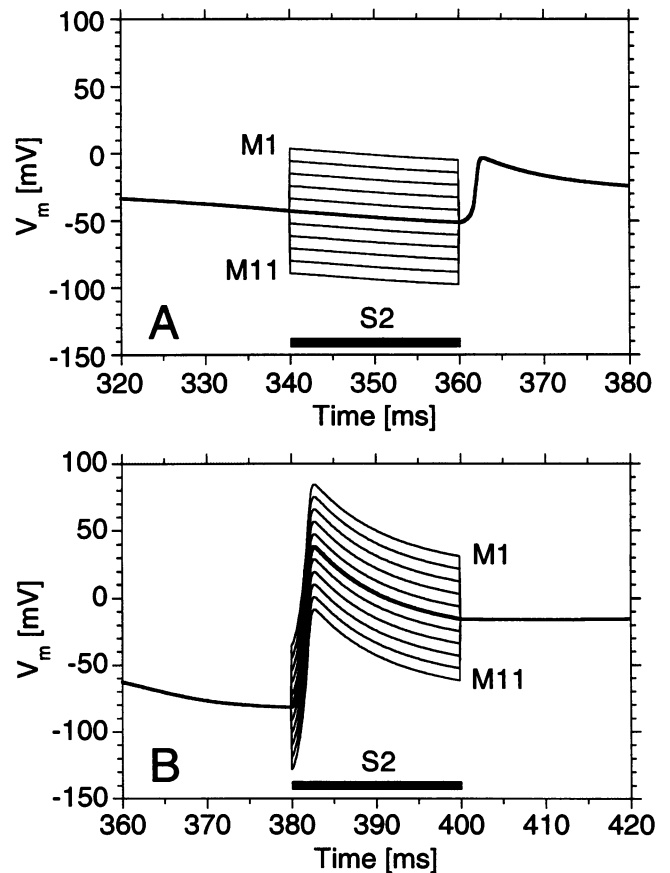

FIGURE 2 Representative excitation responses of all 11 subcellular elements, M1-M11, during two separate field stimulation trials. Otherwise identical 20-ms monophasic stimuli at 2× diastolic threshold were administered to the cell at S1-S2 coupling intervals of (A) 340 ms and (B) 380 ms. The temporal extent of each S2 stimulus is indicated with a horizontal bar. Both examples illustrate the significant separation of transmembrane voltages (V_m) along the cell during (and only during) the S2 stimuli. Furthermore, although both premature stimuli generate new action potentials, in trial A excitation occurs only on S2 release (break), whereas in trial B excitation occurs on S2 onset (make).

spatial nonuniformity of membrane polarizations along the cell length during (and only during) the field stimulus, producing a spatial gradient of potentials ranging from marked depolarization in element M1 to marked hyperpolarization in M11. Furthermore, both S2 stimuli generate new action potentials within the cell. However, as discussed in greater detail below, whereas in trial A the cell fires on the stimulus release (break), in trial B the cell fires on the stimulus onset (make).

Fig. 3 presents recordings of average cellular transmembrane voltage ($\bar{V}_m$) from several similar trials, where S1-S2 coupling intervals range from 330 to 390 ms (in 10-ms increments). The plots have been shifted in time so that all recordings are aligned with respect to the S2 onsets. From these data, we can clearly group the individual plots into three distinct behavioral categories according to the resultant S2 responses: 1) excitation at stimulus make, where a new action potential is elicited at the onset of the stimulus;
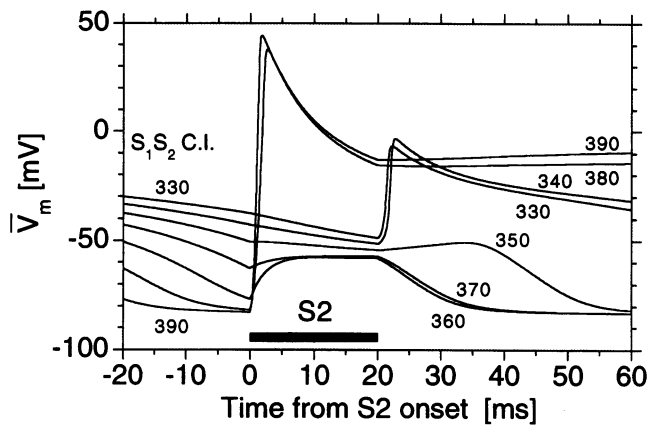
FIGURE 3 Overlaid recordings of average transmembrane voltages ($\bar{V}_{m}$) from trials in which premature, 20-ms, 2× diastolic threshold monophasic S2 stimuli were delivered at S1–S2 coupling intervals of 330 to 390 ms (in 10-ms increments). The plots are cued relative to their S2 onsets (time = 0 ms), with the temporal extent of the coincident S2 stimuli indicated by a horizontal bar. Three distinct excitation response categories can be discerned: excitation on S2 onset (make) for trials involving longer coupling intervals (e.g., 380 and 390 ms), excitation on S2 release (break) for trials involving shorter coupling intervals (e.g., 330 and 340 ms), and no S2 excitation for trials at intervening coupling intervals (e.g., 350, 360, and 370 ms). Note that for trials not inducing make excitation, $\bar{V}_{m}$ are driven toward a field-induced common potential during the S2 stimulus.

2) excitation at stimulus break, where a new action potential is elicited upon the release of the stimulus; and 3) no induced excitation. From Fig. 3, make excitation occurs at relatively long S1–S2 coupling intervals (380 and 390 ms), and break excitation occurs at relatively short S1–S2 coupling intervals (330 and 340 ms). Most surprisingly, how-

ever, is that no excitation occurs at the intervening coupling intervals (350–370 ms).

The monophasic strength-interval map

Fig. 4 A summarizes the cumulative results obtained with 20-ms MP stimuli at many different combinations of stimulus strength and coupling interval. Stimulus strengths are reported relative to the 20-ms MP diastolic S2 threshold. Because of the importance of sodium current during membrane depolarization, contour lines are used to indicate the total inward transmembrane sodium charge movement (Q_{Na}, in nC/cm^2) induced by the S2 stimulus. Each point thus represents the total integration of induced sodium charge movement during and after an S2 stimulus administered at the specified S1–S2 coupling interval. In a previous study, Fishler et al. (1995) presented analogous strength-interval maps, but with maximum upstroke velocity ($\dot{V}_{max}$) as the dependent variable. However, $\dot{V}_{max}$ is not as robust a measure of cellular activation as is Q_{Na}, because $\dot{V}_{max}$ affords only an instantaneous snapshot of the excitatory response. In contrast, Q_{Na} describes the cumulative excitatory response of the cell to the stimulus and thus includes all parts of the excitation process. Indeed, because the membrane capacitance (C_m) is 1 μF/cm^2, to a first approximation (from $V_{Na} = Q_{Na}/C_m$) these contours also describe the total effective positive increase of transmembrane voltage (in millivolts) produced by this sodium current. In concert with these contour lines, shading is employed to indicate the mode of S2 excitation: dark gray for make excitation, light gray for break excitation, and white for no excitation (defined here as $Q_{Na} < 10$ nC/cm^2).
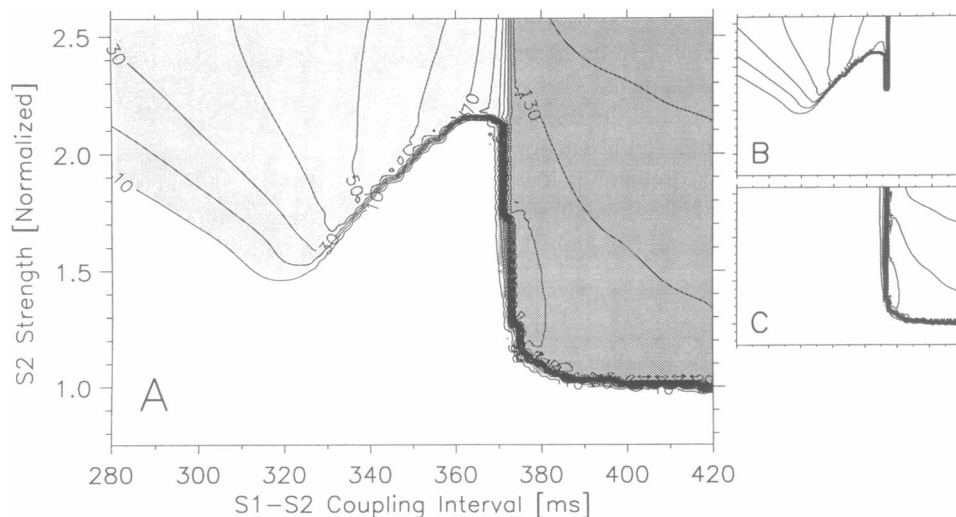

FIGURE 4   (A) Strength-interval map summarizing the excitation responses elicited from an isolated cell by 20-ms monophasic S2 field stimuli of various strengths and S1–S2 coupling intervals. Stimulus strengths are normalized to the monophasic diastolic S2 threshold. Contour lines indicate total inward transmembrane sodium charge movement (Q_{Na} in nC/cm^2) induced by S2. Fills indicate the mode of S2 excitation: dark gray for excitation during S2, light gray for excitation after the end of S2, and white for no excitation (i.e., $Q_{Na} < 10$ nC/cm^2). Note the significant nonmonotonicity of this strength-interval relationship, as well as the sharp "all-or-none" transition at ~372 ms and low field strengths separating the region of no excitation from that of make excitation. (B) Contour map quantifying the amount of Q_{Na} produced only after the end of the S2 stimuli. (C) Contour map quantifying the amount of Q_{Na} produced only during the S2 stimuli. In B and C, axes correspond to those used in A.

There are several features of Fig. 4 *A* worth noting. Most obvious (and as suggested from Fig. 3) is that this MP strength-interval relationship is highly nonmonotonic. Initially, as the S1–S2 coupling interval is shortened from infinity, the threshold for excitation increases—slowly for coupling intervals greater than 380 ms, but then more dramatically near 370–375 ms. However, at 367 ms, this excitation threshold curve reaches a local maximum value of approximately $2.2\times$ diastolic threshold and then decreases for a broad range of coupling intervals before increasing again. It is important to emphasize that this nonmonotonicity is not observed in analogous simulations of stimulation via current injection (Luo and Rudy, 1991), and thus it seems to be a cellular phenomenon elicited only when stimulating with such MP extracellular fields. Furthermore, this behavior is not limited to just the Luo-Rudy (phase 1) model (1991) of cellular electrophysiology. Indeed, we have also documented qualitatively similar nonmonotonic strength-interval relationships when using the Luo-Rudy (phase 2) ventricular (1994), Beeler-Reuter ventricular (1977) (with and without modified Drouhard and Roberge (1987) sodium kinetics), and Earm-Noble atrial (1990) kinetics models (unpublished observations).

Another important feature of the cellular excitatory response illustrated in Fig. 4 *A* is that the sensitivity of this response with respect to S1–S2 coupling interval changes with increasing S2 stimulus strength. At relatively low stimulus strengths, the cell demonstrates an "all-or-none" excitatory response at an S1–S2 coupling interval of $\sim$372 ms—that is, no effective excitation is produced at coupling intervals shorter than 372 ms, but full make excitation occurs at coupling intervals longer than 372 ms. In contrast, at relatively higher stimulus strengths (i.e., $>2.2\times$ diastolic threshold), this strictly all-or-none behavior reverts to a significantly more gradual profile of excitation responses with respect to coupling interval, which is evident in the more widely spaced contour lines of Q_{Na} in Fig. 4 *A*.

Unspecified in Fig. 4 *A* is a clear indication as to when Q_{Na} develops relative to the S2 stimulus. To resolve this ambiguity, Fig. 4, *B* and *C*, illustrates contour maps of the separate contributions to Q_{Na} produced after and during the S2 stimulus, respectively (i.e., break and make responses). There is virtually no overlap in these contributions for MP stimuli—that is, except for a very restricted common region, sodium charge movement occurs either during the stimulus or after it, but not both. Furthermore, the magnitude of Q_{Na} production depends significantly upon the mode of excitation. During make excitation (Fig. 4 *C*), the minimum Q_{Na} is approximately 116 nC/cm^2 and increases in magnitude as either the S1–S2 coupling interval and/or the S2 strength is increased. In contrast, the maximum Q_{Na} during break excitation (Fig. 4 *B*) is only 72 nC/cm^2 and steadily decreases in magnitude as the S1–S2 coupling interval is shortened. Thus, there is a significant discontinuity in Q_{Na} as the mode of excitation changes from make to break, with make excitation always producing far more sodium current than break excitation.

The strength-interval map of Fig. 4 *A* now provides the full context within which to place our observations from Fig. 3 (where S2 strength was $2\times$ diastolic threshold for several coupling intervals). However, this map still fails to explain the mechanisms by which these three modes of excitation operate. To accomplish this, we investigated in much greater detail the spatial and temporal dynamics of the cellular kinetics for three representative S1–S2 coupling intervals at $2\times$ threshold: 340 ms (break excitation), 360 ms (no excitation), and 380 ms (make excitation).

Mechanisms of make excitation by monophasic field stimulus

In general, make excitation only occurs at relatively long S1–S2 coupling intervals (>372 ms in Fig. 3), when sodium kinetics have recovered sufficiently from a previous (S1) action potential so as to supply enough depolarizing current to initiate a new (S2) action potential. We have found that the spatial and temporal dynamics of the sodium activation (m) and inactivation (h and j) gating variables during a field stimulus can fully explain the three modes of excitation. Fig. 5 presents a matrix of panels illustrating how the temporal dynamics of the sodium activation (m, *top row*) and inactivation ($h \cdot j$, *middle row*) gates and their product ($m^3 \cdot h \cdot j$, *bottom row*) evolve at each of the 11 subcellular elements just before and after the onsets of the field S2 stimuli for our three test cases. These results correspond to those traces in Fig. 3 with equivalent S1–S2 coupling intervals.

Just before the delivery of S2 at an S1–S2 coupling interval of 340 ms (Fig. 5, *left column*), the entire cell is isopotential at approximately -43 mV, with all elemental $m \approx 0.5$ and $h \cdot j \approx 0.0$. Upon the onset of S2, however, this isopotential is rapidly lost as elements M5$\rightarrow$M1 are depolarized to increasingly more positive potentials and M7$\rightarrow$M11 are hyperpolarized to increasingly more negative potentials (see Fig. 2 *B*). The sodium gates, in response to these new local transmembrane voltages, are consequently driven toward new, spatially nonuniform values. The elemental m (activation) gates, because of their very small (fast) time constants, rapidly approach their new m_∞ values, which now range almost symmetrically from near 1 at M1–M2 to near 0 at M10–M11 (Fig. 5 *A*). In contrast, most of the elemental $h \cdot j$ (inactivation) gates remain pinned at or near zero, with just the most hyperpolarized element (M11) demonstrating only modest increases (Fig. 5 *B*). However, although most elements of the cell have either m or $h \cdot j$ greater than zero at any particular time instant, none have both quantities simultaneously greater than 0. Thus, each elemental modulation of sodium conductance (as expressed by the product $m^3 \cdot h \cdot j$) remains equal to 0 (Fig. 5 *C*), preventing any production of depolarizing sodium current. Consequently, make excitation is impossible at an S1–S2 coupling interval of 340 ms.

Indeed, for similar reasons, make excitation is also impossible at an S1–S2 coupling interval of 360 ms (Fig. 5,

S1–S2 CI = 340 ms   S1–S2 CI = 360 ms   S1–S2 CI = 380 ms
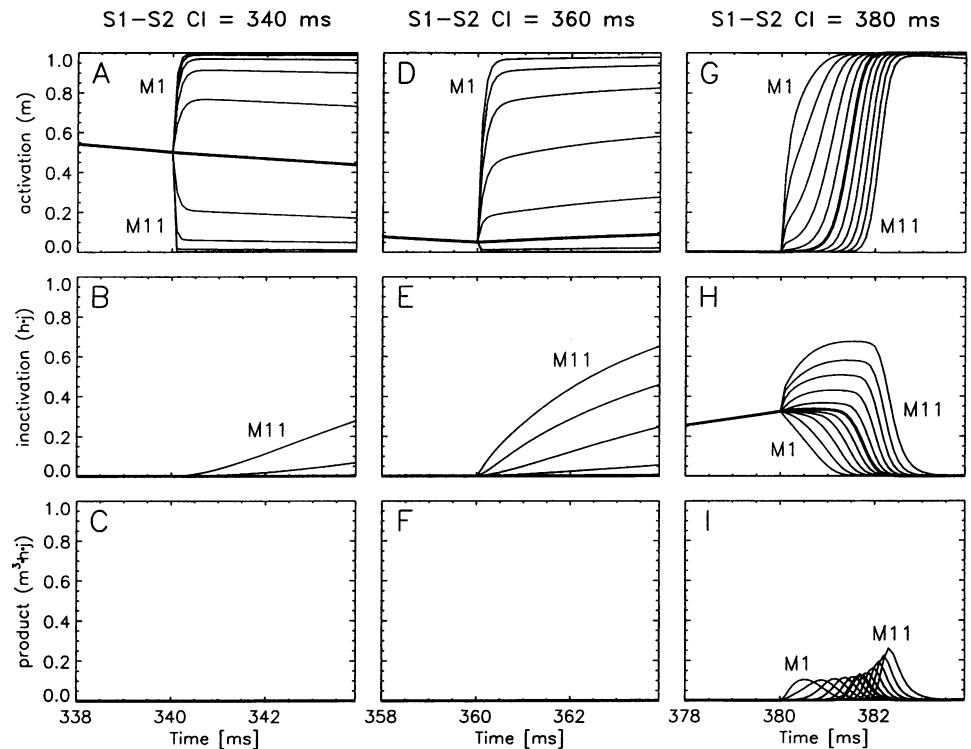
FIGURE 5 Matrix of panels illustrating the separate subcellular (M1–M11) evolutions of the temporal dynamics of sodium activation (m, *top row*) and inactivation ($h \cdot j$, *middle row*) gates, and their product ($m^3 \cdot h \cdot j$, *bottom row*), upon the *onsets* of monophasic S2 field stimuli delivered at S1–S2 coupling intervals of 340 ms (*left column*), 360 ms (*middle column*), and 380 ms (*right column*). All S2 stimuli were 20 ms in duration and 2× diastolic threshold. The temporal evolution of the cell's central membrane patch (M6) is shown with a thickened line. See text for full analysis of these plots.

middle column). Because this coupling interval is 20 ms longer than that of the case above, the cell has had that much more time to repolarize, now to a pre-S2 potential of about −63 mV (see Fig. 3). At this potential, m has almost completely recovered to its resting state (~0; Fig. 5 D), and $h \cdot j$ is still very near zero (Fig. 5 E). As in the case of 340 ms, upon onset of S2, the m within the depolarized half of the cell reactivate to differing degrees toward 1, whereas the products $h \cdot j$ all remain at 0. In contrast, the m within the hyperpolarized half of the cell are rapidly and fully reset to 0, whereas the products $h \cdot j$ are slowly driven to intermediate values greater than 0. Nevertheless, all products of $m^3 \cdot h \cdot j$ remain very near 0 (Fig. 5 F), so that no appreciable sodium current is generated within any of the 11 cellular elements. Thus, as in the case of 340 ms, make excitation cannot occur at this coupling interval either.

The results are quite different, however, when S2 is administered at an S1–S2 coupling interval of 380 ms (Fig. 5, *right column*). By this time, the cell has almost fully repolarized from its S1 action potential to a pre-S2 potential of approximately −80 mV (see Fig. 3). And while sodium activation (m) has fully recovered (= 0; Fig. 5 G), sodium inactivation ($h \cdot j$) has now partially recovered to a pre-S2 value of about 0.3 (Fig. 5 H). During S2, because the time constant for changes to m is so much smaller (faster) than the time constants for both h and j, a significant overlap within the most depolarized regions of the cell is induced where m and $h \cdot j$ are both greater than 0. Consequently, the products $m^3 \cdot h \cdot j$ here are nonzero (Fig. 5 I) and result in a localized nonzero sodium conductance that leads to a large localized inward sodium current. But although localized,

this inward current nevertheless incrementally depolarizes the entire cell. Consequently, m_∞ values increase toward 1 and h_∞ and j_∞ values decrease toward 0. However, because τ_m is still so much smaller (faster) than either τ_h or τ_j, m responds quickly to the increases in m_∞, whereas $h \cdot j$ takes much longer to adjust. Therefore, the products $m^3 \cdot h \cdot j$ slowly increase in magnitude along the cell, further increasing elemental sodium currents and thus further depolarizing the entire cell. Such depolarization is the start of a spatially cascading forward-feedback behavior (see Fig. 5 I), in which the membrane elements activate sequentially along the cell length from M1 to M11 (much like a "domino effect") to rapidly and fully depolarize the entire cell. Thus, this description is the essence of make excitation as generated by a field stimulus and is fundamentally different from that obtained via a current injection protocol (in which the entire cell depolarizes simultaneously).

Mechanisms of break excitation by monophasic field stimulus

Using an approach analogous to that used above to determine the mechanism of make excitation, we plot in Fig. 6 the spatial and temporal dynamics of m, $h \cdot j$, and $m^3 \cdot h \cdot j$ just before and after the break of the same three 20-ms MP S2 field stimuli that were analyzed in Fig. 5.

At an S1–S2 coupling interval of 340 ms, the break of the stimulus occurs at 360 ms (Fig. 6, *left column*). $\bar{V}_m$ just before the break has become more negative since the onset of the stimulus, declining from −43 mV to −52 mV (see Fig. 3 and below). Consequently, m for M6 has decreased
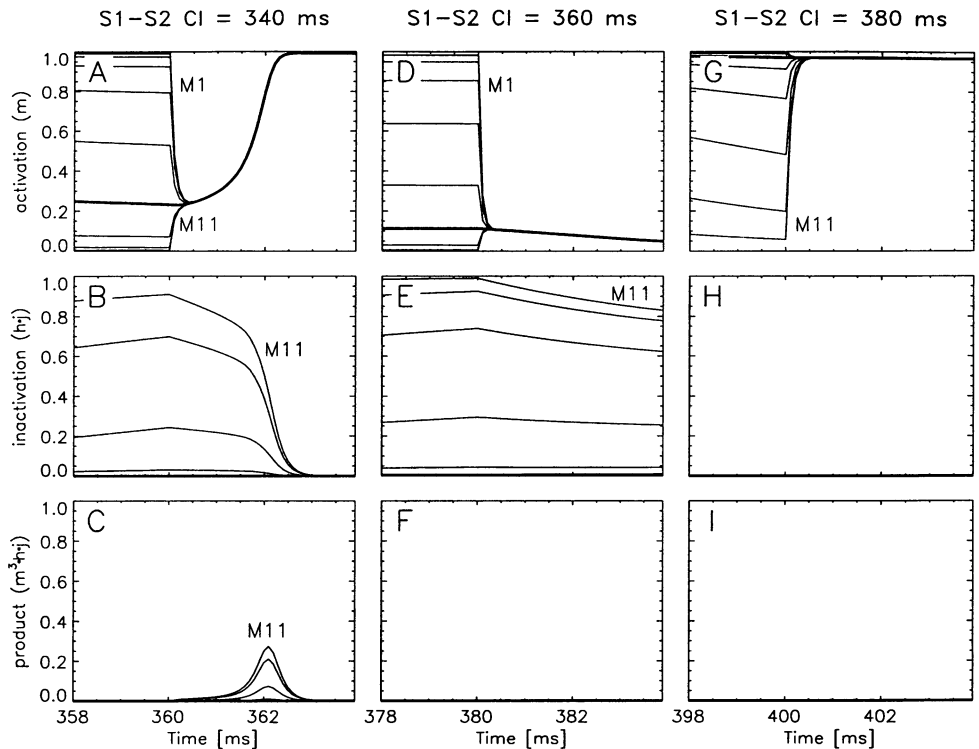
FIGURE 6 Matrix of panels illustrating the separate subcellular (M1–M11) evolutions of the temporal dynamics of sodium activation (m, *top row*) and inactivation ($h \cdot j$, *middle row*) gates, and their product ($m^3 \cdot h \cdot j$, *bottom row*), upon the *release* of monophasic S2 field stimuli originally delivered at S1–S2 coupling intervals of 340 ms (*left column*), 360 ms (*middle column*), and 380 ms (*right column*). All S2 stimuli were 20 ms in duration and 2× diastolic threshold. The temporal evolution of the cell's central membrane patch (M6) is shown with a thickened line. See text for full analysis of these plots.

from ~0.5 at stimulus make (Fig. 5 *A*, *heavy line*) to ~0.25 just before stimulus break (Fig. 6 *A*, *heavy line*), with the values of the other elemental m gates falling in kind. In contrast, $h \cdot j$ remain near 0, except at the hyperpolarized end of the cell, where M9–M11 continue to increase slowly to significantly nonzero values. Upon release of the field stimulus, the spatial gradient in V_m rapidly dissipates and the cell returns to isopotentiality. Thus, $m_\infty \approx 0.25$ and $h_\infty = j_\infty \approx 0.05$ for all elements immediately after stimulus break. However, as in make excitation, the large difference between the activation and inactivation time constants plays a crucial role in the development of break excitation. In that half of the cell that was depolarized by S2 (i.e., M1–M5), the m rapidly fall from larger values toward the new m_∞, whereas the products $h \cdot j$ remain near 0. Thus, the products $m^3 \cdot h \cdot j$ remain at or near 0. In contrast, in the half of the cell that was hyperpolarized by S2 (i.e., M7–M11), the m rapidly rise from near zero toward m_∞, while the products $h \cdot j$ fall only very slowly toward zero. Thus, the products $m^3 \cdot h \cdot j$ (particularly within M9–M11) become significantly greater than 0 (Fig. 6 *C*), and localized inward sodium current can be generated. As in make excitation, this inward current incrementally depolarizes the entire cell, which in turn incrementally increases m_∞ (and slightly decreases h_∞ and j_∞). Again, because of the differences in activation and inactivation time constants, these $m^3 \cdot h \cdot j$ grow in magnitude, thus further increasing the amount of depolarizing inward sodium current through these elements. This positive-feedback system continues to amplify its own signal until eventual excitation. However, unlike the behavior seen during make excitation, the generation of sodium current

during break excitation does not cascade element-to-element down the length of the cell. Rather, it remains localized to those elements for which $h \cdot j$ was significantly greater than 0 at S2 break, which, in this case, are only M9–M11 (Fig. 6 *B*). Consequently, much less total sodium current can be generated during break excitation than is generated during make excitation (see Fig. 4), resulting in slower action potential upstroke velocities (Fishler et al., 1995) as well as lower peak action potential amplitudes (see Fig. 3).

The electrophysiological status of the cell just before the release of the S2 stimulus originally delivered with an S1–S2 coupling interval of 360 ms (Fig. 6, *middle column*) is initially quite similar to that seen for 340 ms, except that now four of the most hyperpolarized elements (M8–M11) demonstrate significantly nonzero values for $h \cdot j$. During this S2, $\bar{V}_m$ increases slightly from −63 mV to −57 mV (see Fig. 3), thereby having only minimal impact on the sodium gating parameters. Just after S2 break, $m_\infty \approx 0.11$ and $h_\infty = j_\infty \approx 0.10$ for all elements. However, compared with the case at an S1–S2 interval of 340 ms, the magnitudes of the $m^3 \cdot h \cdot j$ after the break of S2 are closer to 0, primarily because of the significantly lower value of the m gate (0.11 versus 0.25) and the cubic dependence on m. The resultant reduction in inward current is so severe that it now fails to depolarize the cell enough to initiate the forward-feedback behavior toward excitation. Thus, break excitation fails to ensue.

With the field stimulus delivered at an S1–S2 coupling interval of 380 ms, break excitation is not expected because the cell was already stimulated to excitation on the make of

this S2 (see previous section and Fig. 5, *right column*). Indeed, as seen in Fig. 6 *H*, the products $h \cdot j$ for all elements of the cell are 0 (inactivated) both before and after the break of this S2. Thus, $m^3 \cdot h \cdot j$ also remains 0 and thereby prevents any further sodium current generation.

Reasons for the intervening zone of no excitation

Fig. 3 demonstrates the existence of a range of coupling intervals (350–370 ms) during which no excitation could be elicited, even though field stimuli at both longer and shorter coupling intervals readily excite the same cell. This phenomenon only occurs when the stimulus strength is within the range of values that cuts across the nonmonotonic portions of the MP strength-interval map. For MP stimuli of 20 ms duration (Fig. 4 *A*), this range is seen to be approximately 1.5× to 2.2× the diastolic threshold, with the lower limit not well defined because of the graded response of the cell at the short coupling intervals involved.

The reasons leading to this zone of inexcitability can be distilled from the behavior of the cell during the S2 stimulus delivered at 360 ms (see Figs. 5 and 6, *middle columns*) and can be summarized as a combination of two primary factors: a) the inactivation gates ($h \cdot j$) have not yet sufficiently reactivated toward 1 by the onset of S2 (a necessary condition for make excitation); and b) the activation gate (m) has not remained sufficiently elevated above 0 by the release of S2 (a necessary condition for break excitation). In both of these cases, the total product $m^3 \cdot h \cdot j$ (and thus the total inward sodium current generated) remains at or near 0. Therefore, no excitation is achieved.

Origin of the field-induced common potential

Further study of Fig. 3 reveals that, for all coupling intervals not inducing make excitation, the $\bar{V}_m$ during the S2 stimulus tend to converge toward a common partially depolarized transmembrane potential (in this case, approximately −56 mV). To uncover the source of this field-induced common potential (FICP) response, we analyzed the spatial and temporal behaviors of each of the six transmembrane ionic currents that make up the Luo-Rudy (phase 1) model of membrane dynamics (Luo and Rudy, 1991). We discovered that the current primarily responsible for FICP is the time-independent potassium current I_{K1}. In fact, except at longer S1–S2 coupling intervals during which sodium also makes a significant contribution (e.g., 370 ms in Fig. 3), the behavior of I_{K1} can account for more than 80% of the observed changes in $\bar{V}_m$. Other currents show only minor deviations from their original (unstimulated) kinetics.

I_{K1} is highly inwardly rectifying (Luo and Rudy, 1991), with small-magnitude outward (hyperpolarizing) currents generated for potentials positive to −87.88 mV, and increasingly larger inward (depolarizing) currents generated for potentials negative to −87.88 mV. During a field stimulus, the induced spatial spectrum of potentials (e.g., Fig. 2 *A*) translates into an equivalent spatial spectrum in I_{K1}: I_{K1}

will be large and inward in those regions of the cell hyperpolarized more negative than −87.88 mV, whereas I_{K1} will be small and outward in those regions of the cell depolarized more positive than −87.88 mV. The spatial sum of these regional I_{K1} ($\hat{I}_{K1}$) then controls (in part) the net changes in $\bar{V}_m$: when $\hat{I}_{K1}$ is inward, the cell will depolarize, and conversely, when $\hat{I}_{K1}$ is outward, the cell will hyperpolarize. As time progresses during the stimulus and the cell depolarizes or hyperpolarizes, the spatial spectrum of I_{K1} (and hence $\hat{I}_{K1}$) changes accordingly. But because relatively positive potentials are driven more negative and relatively negative potentials are driven more positive, all $\bar{V}_m$ are driven asymptotically toward a common potential—the potential at which $\hat{I}_{K1} = 0$. For Fig. 3, in which the stimulus strength is 2× diastolic threshold, this field-induced common potential is approximately −56 mV. However, the value of this common potential is a function of the applied field strength and cell geometry (not shown). Increased field strengths lead to a steeper spatial gradient in transmembrane potentials, thereby increasing the breadth of the region subtended on a I_{K1}–V_m curve. But because of the severe inward rectification of I_{K1}, there is now even greater net inward current through I_{K1}, which subsequently induces greater net cellular depolarization to reach the new steady state where $\hat{I}_{K1} = 0$. Consequently, the value of the FICP increases toward more positive values for stronger field stimuli.

Biphasic field stimulation

During BP field stimulation, the extracellular stimulus is divided into two distinct phases of opposite polarities. Fig. 7 presents recordings of $\bar{V}_m$ from several simulations during which a 20-ms total duration BP S2 stimulus (10 ms each phase) at 2× diastolic threshold was administered at S1–S2 coupling intervals ranging from 330 to 390 ms. As in Fig. 3, these plots have been shifted in time so that their S2 shocks coincide. In sharp contrast to its response to MP stimuli, this cell was depolarized, to various degrees, by all of these premature BP stimuli. At the longer S1–S2 coupling intervals (e.g., 380 and 390 ms), the cell activated on the stimulus make, whereas at shorter coupling intervals (e.g., ≤370 ms), the cell responded in a coupling-interval-dependent graded manner to both phasic breaks. Thus, the cellular electrophysiological responses to these BP stimuli seem much less distinct than those observed for the equivalent MP stimuli (cf. Fig. 3).

The biphasic strength-interval map

Fig. 8 *A* summarizes the cellular response to various combinations of 10/10-ms BP S2 stimulus strengths and S1–S2 coupling intervals. As in Fig. 4 *A*, three shades of gray are used to differentiate the modes of excitation, although now with a slight generalization of their definitions: dark gray for excitation during the first phase of the stimulus (i.e.,
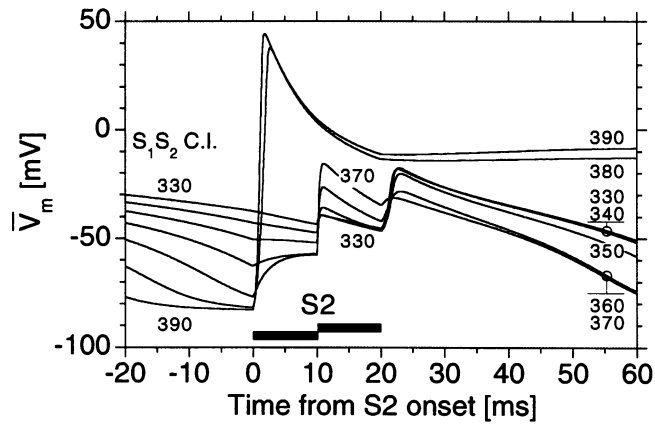
FIGURE 7 Overlaid recordings of average transmembrane voltages ($\bar{V}_m$) from trials in which premature, 10/10 ms, 2× diastolic threshold biphasic S2 stimuli were delivered at S1–S2 coupling intervals of 330 to 390 ms (in 10-ms increments). The plots are cued relative to their S2 onsets (time = 0 ms), with the temporal extent of each phase of the coincident S2 stimuli indicated by a split horizontal bar. As in the monophasic trials, make excitation occurs at relatively long coupling intervals (e.g., 380 and 390 ms). However, unlike the monophasic trials, partial excitation occurs in a coupling-interval-dependent manner at both the transphasic and the break edges of the biphasic stimuli, resulting in at least partial cellular depolarization at all premature coupling intervals.

inward transport of sodium charge (Q_{Na}) induced by these BP stimuli. A complementary strength-interval map in terms of $\dot{V}_{max}$ has been presented previously (Fishler et al., 1995).

A comparison between the MP strength-interval map of Fig. 4 A and the BP strength-interval map of Fig. 8 A reveals several similarities as well as a few important differences. The BP diastolic threshold is only slightly lower than its MP counterpart (0.94 versus 1.00, respectively; Tung and Borderies, 1992). Furthermore, the regions of make excitation are nearly identical, and the graded behavior of Q_{Na} at S1–S2 coupling intervals shorter than ~340 ms also remain quite similar, supporting the notion that the two phases of the BP stimulus act synergistically (Tung and Borderies, 1992). The major differences between these two maps are observed at coupling intervals between ~340 and ~372 ms and are functionally quite significant. Within this interval, the BP waveform extends cellular excitability across the original all-or-none barrier at 372 ms to much shorter coupling intervals than is achievable with equivalent low-strength MP waveforms. Moreover, this additional excitability is graded, such that the induced cellular response (Q_{Na}) now gradually diminishes to 0 as the S1–S2 coupling interval is continually shortened. In the process, this additional excitability effectively removes most of the nonmonotonicity from the original (MP) strength-interval threshold curve.

Fig. 8, B, C, and D, details, respectively, the separate contributions to Q_{Na} produced by the three major divisions

stimulus make), medium gray for excitation after the first phase (i.e., transphasic or break excitation), and white for no appreciable excitation (i.e., $Q_{Na} < 10$ nC/cm^2). Furthermore, as in Fig. 4, contour lines are used to indicate the total
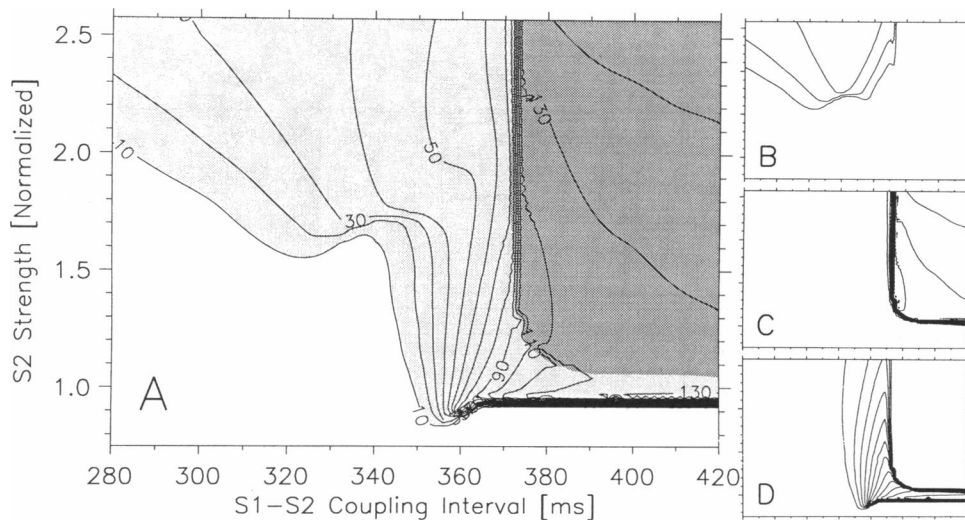

FIGURE 8 (A) Strength-interval map summarizing the excitation responses elicited from an isolated cell by 10/10 ms symmetric biphasic S2 field stimuli of various strengths and S1–S2 coupling intervals. Stimulus strengths are normalized to the monophasic diastolic S2 threshold. Contour lines indicate total inward transmembrane sodium charge movement (Q_{Na} in nC/cm^2) induced by S2. Fills indicate the mode of S2 excitation: dark gray for excitation during the first phase of S2, light gray for excitation after the first phase of S2, and white for no excitation (i.e., $Q_{Na} < 10$ nC/cm^2). In comparison to equivalent monophasic responses in Fig. 4 A, low-strength biphasic stimulation extends cellular excitability to significantly shorter coupling intervals and, in the process, essentially removes the severe nonmonotonicity in the strength-interval relationship. Moreover, this additional excitability transforms the monophasic-induced all-or-none excitation discontinuity into a more gradual, and thus less severe, transition in excitation performances. (B) Contour map quantifying the amount of Q_{Na} produced only after the end of the S2 stimuli. (C) Contour map quantifying the amount of Q_{Na} produced only during the first phase of S2. (D) Contour map quantifying the amount of Q_{Na} produced only during the second phase of S2. In B, C, and D, axes correspond to those used in A.

of the BP S2 stimulus: after the end of S2 (i.e., break response), during the first phase of S2 (i.e., make response), and during the second phase of S2 (i.e., transphasic response). From these separate contour maps it becomes apparent that most of the new features of the BP strength-interval map can be attributed to the transphasic response alone (Fig. 8 *D*): it is the source of charge that converts the all-or-none barrier into a graded transition of excitability, it lowers the BP diastolic threshold below the MP diastolic threshold, it introduces a small region of supernormal excitability at ~357 ms, and it modulates the magnitude of the subsequent break response (compare Fig. 8 *B* to Fig. 4 *B*). Increased charge development during the transphasic response effectively reduces the ability for charge development during the subsequent break response. Thus, whereas the magnitude of the MP break response increases monotonically as the S1–S2 coupling interval is lengthened, the magnitude of the BP break response first increases and then decreases as more charge is developed during the previous transphasic response. As such, the maximum Q_{Na} during BP break excitation (for S2 strengths $\leq 2.6\times$ diastolic threshold) is only 33 nC/cm^2. In contrast, the BP make response (Fig. 8 *C*) remains quite similar both qualitatively and quantitatively to its MP counterpart (Fig. 4 *C*), with only a slight elevation in the diastolic make threshold (1.05 versus 1.00, respectively), due to the relatively shorter make duration (10 ms versus 20 ms).

As in the case with MP stimuli, the detailed spatial and temporal dynamics of the cellular kinetic responses to BP waveforms were examined for three representative BP stimuli delivered at 2$\times$ (MP) diastolic threshold and with S1–S2 coupling intervals of 340, 360, and 380 ms.

Mechanisms of make excitation by biphasic field stimulus

The mechanisms of make excitation by BP field stimuli are essentially identical to those responsible for make excitation by MP field stimuli. This follows from the fact that the first phase of a BP stimulus is identical to the first half of an equivalent MP stimulus. And because, during make excitation, the cell is responding to the onset of the stimulus, these mechanisms must then be identical.

Mechanisms of transphasic excitation by biphasic field stimulus

To determine the mechanisms of transphasic excitation by BP field stimuli, we again studied the spatial and temporal dynamics of sodium activation and inactivation kinetics. Fig. 9 presents plots of m (*top row*), $h \cdot j$ (*middle row*), and $m^3 \cdot h \cdot j$ (*bottom row*) just before and after the phase reversals of BP stimuli delivered at S1–S2 coupling intervals of 340 ms (*left column*), 360 ms (*middle column*), and 380 ms (*right column*).

For S2 delivered at the S1–S2 coupling interval of 340 ms, the stimulus phase reversal occurs at 350 ms (Fig. 9, *left column*). Before this reversal, the cell continues to be influenced by the spatial transmembrane voltage gradient induced by the original extracellular field. The elemental activation (m) gates are distributed between 0.0 at M11 and 1.0 at M1, with M6 at ~0.35. Meanwhile, the elemental inactivation ($h \cdot j$) gates remain highly skewed, with only M9–M11 slowly increasing to values significantly larger than 0. Upon phase reversal at 350 ms, the spatial gradient in V_m rapidly reverses in polarity, such that what was
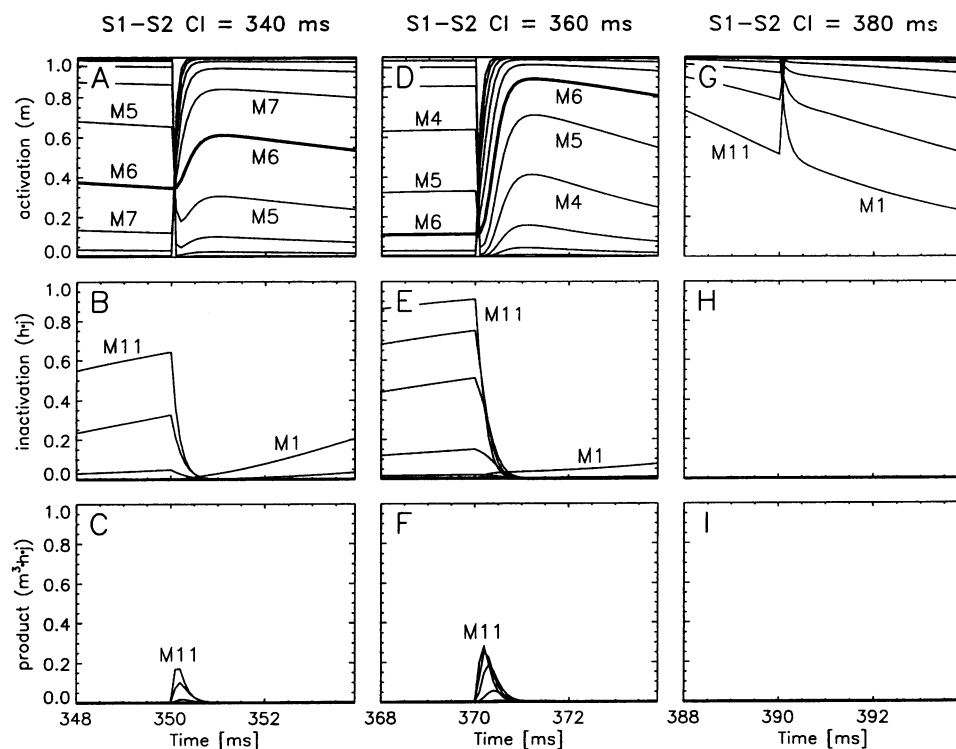

FIGURE 9   Matrix of panels illustrating the separate subcellular (M1–M11) evolutions of the temporal dynamics of sodium activation (m, *top row*) and inactivation ($h \cdot j$, *middle row*) gates, and their product ($m^3 \cdot h \cdot j$, *bottom row*), upon the phase reversal of biphasic S2 field stimuli originally delivered at S1–S2 coupling intervals of 340 ms (*left column*), 360 ms (*middle column*), and 380 ms (*right column*). All S2 stimuli were 10/10 ms symmetric biphasic fields at 2$\times$ monophasic diastolic threshold. The temporal evolution of the cell's central membrane patch (M6) is shown with a thickened line. See text for full analysis of these plots.

previously the hyperpolarized end of the cell is now the depolarized end and vice versa, immediately influencing the sodium gate infinity values and time constants. For example, element M11, which was maximally hyperpolarized during the first phase of the BP stimulus, had $m \approx 0.0$ (Fig. 9 A) and $h \cdot j$ increasing toward 0.65 (Fig. 9 B). Upon phase reversal, M11 is now relatively depolarized, and thus m is rapidly driven toward 1.0 while $h \cdot j$ is driven toward 0.0. The other elements of the cell undergo similar changes to their sodium gates (see Fig. 9, A and B). However, because the sodium inactivation time constants are significantly longer than the activation time constants, M9–M11 experience a brief period of time during which both m and $h \cdot j$ are nonzero, resulting in a transient but significant inward current flow (see Fig. 9 C).

The magnitude of this inward sodium current upon phase reversal is even greater when the BP stimulus is administered at ever longer S1–S2 coupling intervals. The middle column of Fig. 9 presents analogous plots of elemental m, $h \cdot j$, and $m^3 \cdot h \cdot j$ dynamics before and after the phase reversal of a BP stimulus given at an S1–S2 coupling interval of 360 ms. Because the stimulus is 20 ms later, the cell is more repolarized and inactivation recovery has progressed further, such that more elements (M8–M11) have $h \cdot j$ values significantly greater than zero at the time of phase reversal. This translates into a larger total inward sodium current during the period of gating reorientation (see Fig. 9 F), and thus a larger change in $\bar{V}_m$ (see Fig. 7).

No additional sodium current is produced, however, under stimulus conditions where the cell had already fully activated on the stimulus make. Thus, for example, when S2 is delivered with an S1–S2 coupling interval of 380 ms (Fig. 9, right column), complete and sustained sodium inactivation after make excitation prevents further sodium current induction.

Mechanisms of break excitation by biphasic field stimulus

The mechanisms of break excitation by a BP field stimulus are similar to those involved in break excitation by a MP stimulus. However, because a BP shock involves a mid-stimulus phase reversal, the resultant effects on the cell are spatially reversed from those seen during MP break excitation. Furthermore, as described above, $\bar{V}_m$ of this cell has already been influenced in some graded manner by transphasic excitation. Thus, depending on the magnitude of the induced transphasic depolarization, the cell is at a different $\bar{V}_m$ upon break as compared with the break of a comparable MP stimulus. Moreover, the magnitude of the inward sodium current upon the release of S2 is a function of the S1–S2 coupling interval and occurs in a graded manner that is inversely related to the graded response seen upon phase reversal. Thus, for very premature S2s (e.g., S1–S2 coupling interval of 330 ms), there is a very small depolarizing response upon phase reversal and a larger response upon stimulus break (see Fig. 7). Conversely, for S2s delivered at longer coupling intervals (e.g., 370 ms), the

transphasic response is large and the break response is much smaller (see Fig. 7). The mechanisms responsible for this graded break response are similar to those described previously for both MP break and BP transphase excitations and are primarily related to the spatial distribution and magnitudes of the sodium inactivation gates at the time of the stimulus release (not shown).

Effect of stimulus duration on strength-interval relationships

The results described above were all derived from simulations in which the MP and BP S2 field stimuli were 20 ms in total duration. Other S2 durations demonstrated qualitatively similar behaviors and mechanisms. For example, Fig. 10 presents a series of strength-interval map pairs constructed for MP and BP S2 stimuli of 2, 5, 10, and 20 ms total duration. The maps from this latter pair of 20 ms MP and 10/10 ms BP S2 stimuli are identical to those maps illustrated in Figs. 4 A and 8 A, respectively, and are included here for completeness and comparison. The methods of shading and contouring are also identical to those described previously. All strengths have been normalized to the MP diastolic thresholds appropriate for the particular duration of S2. For total durations of 2, 5, 10, and 20 ms, these MP diastolic thresholds were, respectively, 3.71, 3.10, 2.80, and 2.66 V/cm. We hypothesize that these thresholds are higher than those found experimentally (Tung et al., 1991) because (among other reasons) of the idealized streamlined shape of these simulated cells. More typical cell shapes (e.g., cylindrical) and axial nonsymmetries would both introduce increased local surface voltage gradients and result in correspondingly lower threshold values.

Note from Fig. 10 that all MP stimuli, regardless of duration, demonstrate significantly nonmonotonic strength-interval relationships, with persistent all-or-none sensitivities to changes in S1–S2 coupling intervals at relatively low field strengths. The S2 duration does, however, modulate the "width" and "height" of the observed nonmonotonic window of inexcitability: decreasing S2 duration narrows the width but increases the height of this window, although these dependencies are not linear. Analogously, all BP stimuli, regardless of duration, demonstrate essentially monotonic strength-interval relationships with almost universally graded sensitivities to changes in S1–S2 coupling intervals at all suprathreshold field strengths. An exception occurs at the shortest BP stimulus tested (i.e., 1/1 ms BP), where this graded response degenerates slightly into a weak all-or-none response for very low field strengths.

Furthermore, these results confirm that most of the observed premature break responses truly are break-induced excitations rather than delayed make excitations (Knisley et al., 1992b; Krassowska et al., 1992). With delayed excitation, one would expect that the "make" or "break" classification would be sensitive to the stimulus duration. However, we found that break-classified excitations were almost

FIGURE 10 Strength-interval maps for rectangular monophasic and symmetric biphasic S2 field stimuli of 2, 5, 10, and 20 ms total duration. Contour lines and fills are identical to those used in Figs. 4 *A* and 8 *A*. Direct comparisons reveal that both the nonmonotonicity and all-or-none features of the monophasic strength-interval maps persist across all S2 durations tested, with the "width" and "height" of the inexcitable window modulated by the S2 duration. Analogously, the graded response feature of the biphasic strength-interval maps persists for all but the shortest S2 durations tested.
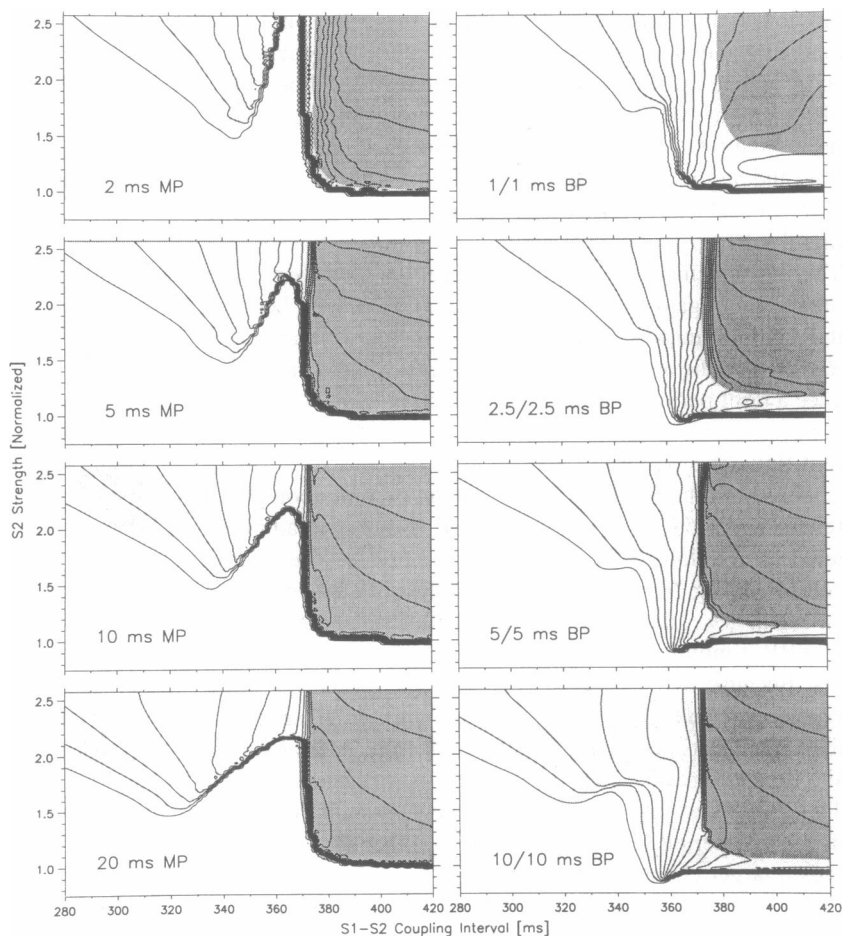
always induced only upon release of the stimulus (or first phase for some BP stimuli), regardless of the stimulus duration. The exceptions can be discerned most easily in the 2-ms MP map as a narrow swath of light gray sandwiched between the zones of make excitation (dark gray) and no excitation (white). In this narrow region, these combinations of stimulus strength and coupling interval induce make excitations, but with latencies that extend beyond the trailing edge of S2 and thus are misclassified as break-induced excitations. Similar swaths can be found for the longer duration stimuli as well, but they are so narrow as to be essentially undetectable. Analyses of excitation mechanisms (e.g., Figs. 5, 6, and 9) corroborate these conclusions.

DISCUSSION

This modeling study presents a thorough description of the multiple mechanisms of excitation involved during the field stimulation of isolated cardiac cells with both MP and BP premature stimuli of various durations. Our simulations and analysis are based on kinetics for ventricular myocytes as described by Luo and Rudy (1991); however, we have found that these results are generalizable to several other myocyte models as well (Beeler and Reuter, 1977; Drouhard and Roberge, 1987; Earm and Noble, 1990; Luo and

Rudy, 1994). These simulation data lend further support to and mechanistic elucidation of two findings recently reported by Fishler et al. (1995). The first is that, unlike the monotonic relationship found during otherwise similar current injection protocols (Luo and Rudy, 1991), the isolated cardiac cell demonstrates a significantly nonmonotonic excitatory response threshold to premature MP field stimuli. The second major finding is that, unlike the observed all-or-none sensitivity to stimulus timing of the MP stimulus excitatory response at relatively low field strengths, the BP stimulus response remains highly graded across all premature coupling intervals. These and other important results, and their implications, are discussed in greater detail below.

Field stimulation versus current injection

This study presents results obtained from simulations in which a symmetric isolated cardiac cell was stimulated by a uniform extracellular electric field. We consider these geometric and field idealizations to represent limiting cases of the more general case of the excitation of cardiac tissue situated relatively far from any stimulating electrodes. Previous modeling studies of cardiac tissue excitation have predicted that the transmembrane potentials induced by such a stimulus can be described as the superposition of distinct aperiodic and periodic compo-

nents (Plonsey and Barr, 1986b; Krassowska et al., 1987; Trayanova and Pilkington, 1993). The aperiodic polarizations are largest in magnitude nearest the stimulating electrodes and arise from the necessary redistribution of stimulating currents between the intracellular and extracellular domains. In contrast, the periodic polarizations arise from secondary sources located at the intercellular boundaries (Plonsey and Barr, 1986b). These secondary sources induce a periodic pattern of hyperpolarizations and depolarizations at the cellular scale (Plonsey and Barr, 1986b; Krassowska et al., 1987; Trayanova and Pilkington, 1993). However, these polarizations are generally smaller in magnitude than the aperiodic response and so presumably only become important in regions relatively far from the stimulating electrodes.

Field stimulation of a cell differs significantly from that of intracellular current injection in several important ways. For example, the source of depolarizing current differs considerably between field and current stimulation (Tung and Borderies, 1992; Krassowska and Neu, 1994). Because field stimulation supplies no net current to the cell, all depolarizing currents (e.g., sodium) must be actively generated through the cell membrane. In contrast, intracellular current injection alone can directly supply the necessary current for depolarization, and thus no transmembrane ionic currents need be activated. Furthermore, whereas current injection polarizes the entire membrane uniformly, field stimulation polarizes it nonuniformly, with one end of the cell depolarized and the other end hyperpolarized. These differences in polarization profiles also result in substantial differences in the rapidity with which the cell membrane potentials can respond to such stimuli, with the response under space-clamped conditions substantially slower than that under field conditions (Cartee and Plonsey, 1992; Krassowska and Neu, 1994). Fundamental to this swift response is the ability for charge to rapidly redistribute between the well-coupled, oppositely polarized regions of the cell (Cartee and Plonsey, 1992)—behavior that may be fundamental to the excitatory break response observed with field stimulation. Additional contrasting behaviors between field stimulation and current injection have been identified for resting cells by Tung and Borderies (1992). Consequently, it is doubtful that the superposition of current injection results could accurately reproduce all of the behaviors observed during field stimulation.

The field-induced common potential

While modeling the responses of resting cells to uniform fields, Tung and Borderies (1992) found that I_{K1} (the time-independent inwardly rectifying potassium current) was a major contributor to the initial net depolarization of a cell. We extend this finding here to include other cellular refractory states as well. Our analyses indicate that, except for cells that have been excited on the make of the field stimulus, I_{K1} is the transmembrane current most affected during the stimulus and forces the cellular transmembrane potential ($\bar{V}_m$) during the shock toward the potential at which the net I_{K1} current integrated across the entire cell is near 0. Because I_{K1} is highly inwardly rectifying

(and thus nonlinear with voltage), this potential is usually significantly more positive than the I_{K1} reversal potential. Furthermore, except as noted above, the initial cellular $\bar{V}_m$ is irrelevant—cells from almost all refractory states will be forced toward this common potential. Thus, as illustrated in Fig. 3, such a field stimulus might actually accelerate the repolarization of highly refractory cells.

Monophasic field stimulation

From our simulation results, we note two distinct modes of excitation when administering premature MP field stimuli (see Fig. 4): a) make excitation for relatively long S1–S2 coupling intervals, and b) break excitation for shorter coupling intervals. The mechanisms responsible for these two types of excitation also differ considerably. Make excitation is observed only when the cell has had sufficient time to repolarize to a level where sodium inactivation is at least partially removed before the onset of a stimulus. Under these conditions, the onset of the field stimulus induces sodium activation within the depolarized half of the cell, which then initiates a spatial cascade of inward sodium current generation along the cell that produces full activation. In contrast, break excitation is unmasked only when the S2 stimulus is too premature for make excitation to occur—that is, when sodium inactivation still dominates the cell's sodium kinetics. Under these conditions, the field stimulus does not directly activate the cell, but rather induces a spatial transmembrane voltage gradient along the cell such that one end is relatively depolarized and the other end is relatively hyperpolarized (Klee and Plonsey, 1976; Plonsey and Barr, 1986a; Krassowska et al., 1987; Tung and Borderies, 1992; Leon and Roberge, 1993; Krassowska and Neu, 1994). Whereas the depolarized end of the cell remains highly inactivated during the entire stimulus, the (negative) drop in voltage within the hyperpolarized end induces a relatively rapid local removal of sodium inactivation. Then, when the stimulus ends and the transmembrane voltages rapidly return to isopotentiality, the sudden (positive) increase in voltage within the once-hyperpolarized end of the cell acts as an effective "stimulus" on that membrane region. With sodium inactivation now at least partially removed here from the stimulus itself, sufficient inward sodium current develops to subsequently excite the cell. Note that break excitation cannot be explained by or duplicated with space-clamped current injection stimulation (Hoshi and Matsuda, 1962).

Few experimental data exist that address the excitation responses of cardiac cells exposed to uniform MP and/or BP extracellular electric fields of various strengths and prematurities. The most revealing set is from Knisley et al. (1992a), who performed tissue experiments to quantify the resultant action potential prolongations induced by premature MP field stimuli (2 ms in duration) of various strengths. This quantity is qualitatively correlated to excitation response (Leon and Roberge, 1993; Jones et al., 1994) and thus these should corroborate each other. Indeed, their results demonstrated a distinct all-or-none prolongation response for relatively low shock

strengths (e.g., 2.5 V/cm) and a very gradual prolongation response for higher shock strengths (e.g., 8 V/cm)—qualitative features that agree well with our model results. Dillon and Mehra (1992) obtained similar results using 1-ms defibrillatory shocks of isolated rabbit hearts. Unfortunately, both sets of published data were too sparse to determine conclusively whether their preparations also exhibited a nonmonotonic strength-interval response similar to our model predictions.

There are also intriguing similarities between the non-monotonic strength-interval relationship produced in our MP simulations and the "dip phenomenon" observed in experimentally derived threshold interval curves of Orias et al. (1950) and Dekker et al. (1970). Using unipolar extra-cellular stimulation of canine hearts, these studies clearly demonstrated a nonmonotonic "dip" in their measured composite strength-interval curves. Moreover, analogous to our simulation results, responses at shorter coupling intervals—including this dip region—were associated with (anodal) break excitation, whereas responses at longer coupling intervals were associated with (cathodal) make excitation. However, because of the significant differences between the respective substrates and protocols (e.g., cell versus tissue, uniform field versus unipolar stimulation, etc.), a direct correlation between these computational and experimental results is premature.

Biphasic field stimulation

When BP field stimuli are used instead of the MP stimuli, a dramatically different overall cellular response is observed (Fishler et al., 1995). Whereas the MP stimuli elicited a distinctly nonmonotonic strength-interval excitation threshold relationship, the BP stimuli elicited a fundamentally monotonic relationship. And whereas the cell demonstrated an all-or-none excitatory response to low-strength MP stimuli and a more graded response to higher strength stimuli, the response to the BP stimuli remained graded for all stimulus strengths. So why are there such significant differences between these responses?

One of the major limitations to excitation via MP field stimulation is that unless the cell excites on the stimulus make, less than half of the cell (i.e., only part of the hyperpolarized half) can contribute to the excitation process; the other (depolarized) half remains inactivated and thus fails to assist in cellular depolarization. By introducing a polarity reversal into the field stimulus as in BP stimulation, both halves of the cell can potentially contribute to the depolarization process. Moreover, these contributions are sequential, such that some depolarizing current is generated from one half of the cell after the end of the first stimulus phase, and additional depolarizing current is generated from the other half of the cell after the end of the second stimulus phase. The amount of depolarizing current that each cell half contributes is (at least) a function both of the field strength and of the initial transmembrane voltage at the time of the stimulus onset (itself related to the S1–S2 coupling

interval; see Fig. 8, *B* and *D*). Such synergistic behavior during BP field stimulation was shown previously during diastole (Tung and Borderies, 1992) and more recently for a few earlier refractory states (Leon and Roberge, 1993), and cannot be easily deduced from similar current injection simulations (Jones and Jones, 1990; Jones et al., 1994).

This theory might suggest that adding many polarity reversals into the stimulus would further improve its outcome. However, this extrapolation must be viewed with caution. Once a stimulus has "tapped" each end of the cell for its sodium current contribution and has at least partially depolarized the cell, further reversals might reach a point of diminishing returns. Furthermore, although all of these field stimuli induce cellular current flow upon a change in the field gradient profile (i.e., at either a make, transphasic, or break edge), that current flow does not occur instantaneously. For example, for a 2× threshold stimulus, the transphasic current develops over approximately 1 ms (see Fig. 9, *D* and *F*); for weaker stimuli, the current develops over even longer intervals (e.g., ~8 ms within the super-normal region of Fig. 8 *A*). These intervals are directly related to the local rates of sodium inactivation recovery across the cell. Thus, for a stimulus to be most effective, a field gradient change should be followed by an interval of relative field stability so that the cells can fully react to that new gradient. Therefore, rapid switching of the field polarity (especially at very low field strengths) could conceivably even hamper the development of depolarizing currents. Indeed, such detrimental effects can be observed in the 1/1 ms BP strength-interval map of Fig. 10, where the region of supernormal excitability has disappeared and part of the graded response at low field strengths has degenerated into an all-or-none response.

Implications in defibrillation

Certainly, a single cell does not a heart make. Our model, and the results obtained with it, can offer only a glimpse into the complex electrophysiological interactions that occur during whole-heart defibrillation between the endogenous fibrillatory activity and the exogenous electric field. Nevertheless, careful extrapolation of results can offer new and useful insights into the behaviors of these otherwise complex phenomena. Indeed, Fishler et al. (1995) presented preliminary results from a one-dimensional cardiac strand model exposed to MP and BP field stimuli that at least qualitatively support some of these new ideas.

The objective of modern defibrillation strategies is to achieve successful termination of all fibrillatory activity while using as little energy as possible. Ideally, such a defibrillation shock would employ only the minimum field strength throughout the cardiac volume necessary to halt all propagation wavefronts while also preventing the (re)initiation of new wavefronts (Chen et al., 1991). Unfortunately, because of the complex geometry of the heart and its associated structures, it is impossible to generate these minimum

electric fields simultaneously for all regions of the heart. Instead, some regions will incur higher-than-necessary fields so as to guarantee that this minimum field strength will reach the more distal regions of the heart. Indeed, several studies have demonstrated that unsuccessful defibrillation shocks fail because of continued propagated activity within regions of the heart that experienced the smallest field gradients during the shock (Chen et al., 1986; Shibata et al., 1988; Zhou et al., 1993). Thus, presumably one method for increasing defibrillation success is to improve the efficacy of the shock within the low-field-gradient regions of the heart.

To this end, it has been shown both experimentally (Flaker et al., 1989; Feeser et al., 1990) and clinically (Fain et al., 1989; Winkle et al., 1989) that some (Tang et al., 1989) BP defibrillation shocks are more efficacious than their MP counterparts. However, no study has been able to demonstrate conclusively the mechanism(s) of this improved performance. A leading hypothesis, as proposed by Jones et al. (1994), suggests that the enhanced excitatory response of partially refractory tissue to low-strength BP shocks results in greater refractory period prolongation, which increases the tissue's protection from any potentially refibrillatory wavefronts that might try to penetrate from distal regions. Our simulation results here do not directly address the issue of refractory period prolongation, but rather focus on the mechanisms of the excitatory response itself. Nevertheless, our analysis of this excitatory response does suggest an alternative and/or supplementary hypothesis to explain the potential for increased efficacy of BP defibrillation shocks over equivalent MP shocks.

Recall that during fibrillation, synchronization of cardiac activation is lost, leading to high spatial variability in wavefront and action potential activity: at any given time during fibrillation, one will find multiple, nonstationary, propagating wavefronts coursing through the myocardial volume. Consequently, any defibrillatory shock will interact with these multiple wavefronts and thus encounter cells at all phases of refractoriness. According to our strength-interval results of Fig. 10, a low-strength (i.e., $<1.5\times$ diastolic threshold) MP shock would fully excite cells near diastolic potentials while having practically no effect on the remaining, more refractory cells—that is, a classic all-or-none response. This response would lead to highly depolarized regions of tissue situated adjacent to highly repolarized regions—conditions that are conducive to the reinitiation of propagated activity (Knisley et al., 1992a; Knisley and Hill, 1993). Furthermore, if the shock strength is in the range that cuts through the nonmonotonic section of the strength-interval curve, additional fibrillatory effects could result: two activated regions would develop separated by an unaffected, but nearly repolarized, swath of tissue, thereby doubling the number of potentially refibrillatory wavefronts. In contrast, according to Fig. 10, equivalent low-strength BP shocks, while also fully exciting cells near diastole, would always (except for very short stimuli) have a graded excitatory effect on cells in other more refractory states (i.e., at earlier coupling intervals). Thus, there would never be any steep spatial gradients in transmembrane potentials to sustain and/or generate activating currents for further post-shock propagation. Initial results from computer simulations of the interaction between propagating wave fronts and imposed MP and BP stimuli support some of these predictions (Fishler et al., 1995). Consequently, from these analyses, we propose that the increased defibrillation efficacy of BP waveforms might result from the consistently graded excitatory response of cells to low-strength BP shocks, a feature that is notably absent from the all-or-none response generated by equivalent low-strength MP shocks. Such a graded response would produce at least two significantly antiarrhythmic effects (Knisley et al., 1992a; Knisley and Hill, 1993): 1) it would more effectively depolarize cells from most refractory states, and thus further inactivate them from future reexcitation; and 2) it would result in a more spatially uniform distribution of post-shock transmembrane potentials (compare post-shock potential distributions in Figs. 3 and 7), which would reduce the spatial gradient of transmembrane voltages that could otherwise drive the reinitiation of propagated activity. Although refractory period prolongation could then also afford an additional level of protection from any encroaching propagation wavefronts, we speculate that this added protection might instead be due to the persistence of the graded voltage profile rather than to the duration of the prolongation alone.

Finally, although this paper has focused on the excitation responses of a single isolated cardiac cell within an extracellular field, these results might also apply at slightly larger size scales as well. For example, similar synergistic dynamics could occur between neighboring, well-coupled, but unequally polarized regions of cardiac tissue. Such potential distributions have been demonstrated during point stimulation of cardiac tissue, in which virtual electrode effects produce oppositely polarized yet closely spaced regions of tissue (Knisley et al., 1994; Roth and Wikswo, 1994; Neunlist and Tung, 1995). Furthermore, recent modeling work has demonstrated that whole-heart defibrillation produces large spatial variations in tissue polarizations over relatively short distances (Trayanova and Eason, 1995). However, certain assumptions adopted in these simulations would no longer necessarily apply (e.g., intracellular isopotentiality). Thus, whether these MP and BP dynamics as described herein would be influential under any or all of these supercellular conditions remains an open question for future computational and experimental studies.

REFERENCES

Beeler, G. W., and H. Reuter. 1977. Reconstruction of the action potential of ventricular myocardial fibres. *J. Physiol. (Lond.).* 268:177–210.

Cartee, L. A., and R. Plonsey. 1992. The transient subthreshold response of spherical and cylindrical cell models to extracellular stimulation. *IEEE Trans. Biomed. Eng.* 39:76–85.

Chen, P.-S., N. Shibata, E. G. Dixon, P. D. Wolf, N. D. Danieley, M. B. Sweeney, W. M. Smith, and R. E. Ideker. 1986. Activation during ventricular defibrillation in open-chest dogs: evidence of complete cessation and regeneration of ventricular fibrillation after unsuccessful shocks. *J. Clin. Invest.* 77:810–823.

Chen, P.-S., P. D. Wolf, and R. E. Ideker. 1991. Mechanism of cardiac defibrillation: a different point of view. *Circulation.* 84:913–919.

Dekker, E. 1970. Direct current make and break thresholds for pacemaker electrodes on the canine ventricle. *Circ. Res.* 27:811–823.

Dillon, S. M., and R. Mehra. 1992. Prolongation of ventricular refractoriness by defibrillation shocks may be due to additional depolarization of the action potential. *J. Cardiovasc. Electrophysiol.* 3:442–456.

Drouhard, J. P., and F. A. Roberge. 1987. Revised formulation of the Hodgkin-Huxley representation of the sodium current in cardiac cells. *Comput. Biomed. Res.* 20:333–350.

Earm, Y. E., and D. Noble. 1990. A model of the single atrial cell: relation between calcium current and calcium release. *Proc. R. Soc. Lond.* 240:83–96.

Fain, E. S., M. B. Sweeney, and M. R. Franz. 1989. Improved internal defibrillation efficacy with a biphasic waveform. *Am. Heart J.* 117: 358–364.

Feeser, S. A., A. S. L. Tang, K. M. Kavanagh, D. L. Rollins, W. M. Smith, P. D. Wolf, and R. E. Ideker. 1990. Strength-duration and probability of success curves for defibrillation with biphasic waveforms. *Circulation.* 82:2128–2141.

Fishler, M. G., E. A. Sobie, L. Tung, and N. V. Thakor. 1996. Cardiac responses to premature monophasic and biphasic field stimuli: results from cell and tissue modeling studies. *J. Electrocardiol.* 28:174–179.

Flaker, G. C., J. C. Schuder, W. C. McDaniel, H. Stoeckle, and M. Dbeis. 1989. Superiority of biphasic shocks in the defibrillation of dogs by epicardial patches and catheter electrodes. *Am. Heart J.* 118:288–291.

Gross, D., L. M. Loew, and W. W. Webb. 1986. Optical imaging of cell membrane potential changes induced by applied electric fields. *Biophys. J.* 50:339–348.

Hoshi, T., and K. Matsuda. 1962. Excitability cycle of cardiac muscle examined by intracellular stimulation. *Jpn. J. Physiol.* 12:433–446.

Jones, J. L., and R. E. Jones. 1990. Threshold reduction with biphasic defibrillator waveforms. Role of excitation channel recovery in a computer model of the ventricular action potential. *J. Electrocardiol.* 23: 30–35.

Jones, J. L., R. E. Jones, and G. Balasky. 1987. Improved cardiac cell excitation with symmetrical biphasic defibrillator waveforms. *Am. J. Physiol.* 253:H1418–H1424.

Jones, J. L., R. E. Jones, and K. B. Milne. 1994. Refractory period prolongation by biphasic defibrillator waveforms is associated with enhanced sodium current in computer models of the ventricular action potential. *IEEE Trans. Biomed. Eng.* 41:60–68.

Klee, M., and R. Plonsey. 1976. Stimulation of spheroidal cells—the role of cell shape. *IEEE Trans. Biomed. Eng.* BME-23:347–354.

Knisley, S. B., T. F. Blitchington, B. C. Hill, A. O. Grant, W. M. Smith, T. C. Pilkington, and R. E. Ideker. 1993. Optical measurements of transmembrane potential changes during electric field stimulation of ventricular cells. *Circ. Res.* 72:255–270.

Knisley, S. B., and B. C. Hill. 1993. Optical recordings of the effect of electrical stimulation on action potential repolarization and the induction of reentry in two-dimensional perfused rabbit epicardium. *Circulation.* 88:2402–2414.

Knisley, S. B., B. C. Hill, and R. E. Ideker. 1994. Virtual electrode effects in myocardial fibers. *Biophys. J.* 68:719–728.

Knisley, S. B., W. M. Smith, and R. E. Ideker. 1992a. Effect of field stimulation on cellular repolarization in rabbit myocardium. Implications for reentry induction. *Circ. Res.* 70:707–715.

Knisley, S. B., W. M. Smith, and R. E. Ideker. 1992b. Effect of intrastimulus polarity reversal on electric field stimulation thresholds in frog and rabbit myocardium. *J. Cardiovasc. Electrophysiol.* 3:239–254.

Krassowska, W., C. Cabo, S. B. Knisley, and R. E. Ideker. 1992. Propagation versus delayed activation during field stimulation of cardiac muscle. *Pacing Clin. Electrophysiol.* 15:197–210.

Krassowska, W., and J. C. Neu. 1994. Response of a single cell to an external electric field. *Biophys. J.* 66:1768–1776.

Krassowska, W., T. C. Pilkington, and R. E. Ideker. 1987. Periodic conductivity as a mechanism for cardiac stimulation and defibrillation. *IEEE Trans. Biomed. Eng.* BME-34:555–560.

Leon, L. J., and F. A. Roberge. 1993. A model study of extracellular stimulation of cardiac cells. *IEEE Trans. Biomed. Eng.* 40:1307–1319.

Luo, C.-H., and Y. Rudy. 1991. A model of the ventricular cardiac action potential. Depolarization, repolarization, and their interaction. *Circ. Res.* 68:1501–1526.

Luo, C.-H., and Y. Rudy. 1994. A dynamic model of the cardiac ventricular action potential. I. Simulations of ionic currents and concentrations. *Circ. Res.* 74:1071–1096.

Mirowski, M. 1985. The automatic implantable cardioverter-defibrillator: an overview. *J. Am. Coll. Cardiol.* 6:461–466.

Neunlist, M., and L. Tung. 1995. Spatial distribution of cardiac transmembrane potentials around an extracellular electrode: dependence on fiber orientation. *Biophys. J.* 68:2310–2322.

Orias, O., C. M. Brooks, E. E. Suckling, J. L. Gilbert, and A. A. Siebens. 1950. Excitability of the mammalian ventricle throughout the cardiac cycle. *Am. J. Physiol.* 163:272.

Plonsey, R., and R. C. Barr. 1986a. Effect of microscopic and macroscopic discontinuities on the response of cardiac tissue to defibrillating (stimulating) currents. *Med. Biol. Eng. Comput.* 24:130–136.

Plonsey, R., and R. C. Barr. 1986b. Inclusion of junction elements in a linear cardiac model through secondary sources: application to defibrillation. *Med. Biol. Eng. Comput.* 24:137–144.

Roth, B. J., and J. P. Wikswo, Jr. 1994. Electrical stimulation of cardiac tissue: a bidomain model with active membrane properties. *IEEE Trans. Biomed. Eng.* 41:232–240.

Schuder, J., J. H. Gold, H. Stoeckle, W. C. McDaniel, and K. N. Cheung. 1983. Transthoracic ventricular defibrillation in the 100 kg calf with symmetrical one-cycle bidirectional rectangular wave stimuli. *IEEE Trans. Biomed. Eng.* 30:415–422.

Shibata, N., P.-S. Chen, E. G. Dixon, P. D. Wolf, N. D. Danieley, W. M. Smith, and R. E. Ideker. 1988. Epicardial activation after unsuccessful defibrillation shocks in dogs. *Am. J. Physiol.* 255:H902–H909.

Tang, A. S. L., S. Yabe, J. M. Wharton, M. Dolker, W. M. Smith, and R. E. Ideker. 1989. Ventricular defibrillation using biphasic waveforms: the importance of phasic duration. *J. Am. Coll. Cardiol.* 13:207–214.

Trayanova, N. A., and J. C. Eason. 1995. Shock-induced transmembrane potential distribution in the canine heart: effects of electrode location and polarity. *Pacing Clin. Electrophysiol.* 18:878.

Trayanova, N., and T. C. Pilkington. 1993. A bidomain model with periodic intracellular junctions: a one-dimensional analysis. *IEEE Trans. Biomed. Eng.* 40:424–433.

Tung, L., and J.-R. Borderies. 1992. Analysis of electric field stimulation of single cardiac muscle cells. *Biophys. J.* 63:371–386.

Tung, L., N. Sliz, and M. R. Mulligan. 1991. Influence of electrical axis of stimulation on excitation of cardiac muscle cells. *Circ. Res.* 69:722–730.

Wharton, J. M., V. J. Richard, C. E. Murry, E. G. Dixon, K. A. Reimer, J. Meador, W. M. Smith, and R. E. Ideker. 1990. Electrophysiological effects of monophasic and biphasic stimuli in normal and infarcted dogs. *Pacing Clin. Electrophysiol.* 13:1158–1172.

Windisch, H., H. Ahammer, P. Schaffer, W. Müller, and D. Platzer. 1992. Fast optical potential mapping in single cardiomyocytes during field stimulation. *Proc. IEEE Eng. Med. Biol. Soc.* 14:634–635.

Winkle, R. A., R. H. Mead, M. A. Ruder, V. Gaudiani, W. S. Buch, B. Pless, M. Sweeney, and P. Schmidt. 1989. Improved low energy defibrillation efficacy in man with the use of a biphasic truncated exponential waveform. *Am. Heart J.* 117:122–127.

Zhou, X., J. P. Daubert, P. D. Wolf, W. M. Smith, and R. E. Ideker. 1993. Epicardial mapping of ventricular defibrillation with monophasic and biphasic shocks in dogs. *Circ. Res.* 72:145–160.